Received: 16 November 2017 | Revised: 25 June 2017 | Accepted: 10 July 2018

DOI: 10.1002/mrm.27476

FULL PAPER

Magnetic Resonance in Medicine

A human cerebral and cerebellar 8-channel transceive RF dipole coil array at 7T

Jérémie D. Clément[1] | **Rolf Gruetter**[1,2,3] | **Özlem Ipek**[4]

[1]LIFMET, Ecole Polytechnique Fédérale de Lausanne (EPFL), Geneva, Switzerland

[2]Department of Radiology, University of Geneva, Geneva, Switzerland

[3]Department of Radiology, University of Lausanne, Lausanne, Switzerland

[4]CIBM-AIT, EPFL, Lausanne, Switzerland

Correspondence
Jérémie D. Clément, EPFL SB IPHYS LIFMET, Station 6, 1015 Lausanne, Switzerland.
Email: jeremie.clement@epfl.ch

Purpose: Dipole antennas that provide high transmit field penetration with large coverage, and their use in a parallel transmit setup, may be advantageous in minimizing B_1^+-field inhomogeneities at ultra-high field, i.e 7T. We have developed and evaluated an 8-channel RF dipole coil array for imaging the entire cerebral and cerebellar regions in man.

Methods: A coil array was modeled with seven dipoles: six placed covering the occipital and temporal lobes; one covering the parietal lobe; and two loops covering the frontal lobe. Center-shortened and fractionated dipoles were simulated for the array configuration and assessed with respect to B_1^+-field at maximum specific absorption rate averaged over 10 g tissue regions in human brain. The whole-brain center-shortened dipoles with frontal loops coil array was constructed and its transmit properties were assessed with respect to MR images, B_1^+-field, and homogeneity.

Results: In simulations, the dipole arrays showed comparable performances to cover the whole-brain. However, for ease of construction, the center-shortened dipole was favored. High spatial resolution anatomical images of the human brain with the coil array demonstrated a full coverage of the cerebral cortex and cerebellum.

Conclusions: The 8-channel center-shortened dipoles and frontal loops coil array promises remarkable efficiency in highly challenging regions as the cerebellum, and phase-only RF shimming of whole-brain could greatly benefit ultra-high field magnetic resonance imaging of the human brain at 7T.

KEYWORDS

center-shortened dipole, parallel transmit, radiofrequency coil array, ultra-high field, 7T, whole human brain imaging

1 | INTRODUCTION

At ultra-high field, magnetic resonance (MR) studies benefit from higher signal-to-noise ratio (SNR)[1,2] and better spectral[3] and spatial resolution,[4] compared to lower field MR scanners. However, the shorter wavelength ($\lambda \approx 12$ cm at 7T in the brain) causes noticeable RF inhomogeneity and decreased RF penetration of human tissues.[5] Furthermore, the rise in tissue temperature during RF excitation can be higher, as the requirements for energy of RF pulses generally scale

with frequency.[6–8] For these reasons, there are three general challenges when working at ultra-high field: increased RF inhomogeneity, limited RF penetration and high energy deposition in tissues. At lower fields, i.e 1.5T and 3T, limited RF penetration and inhomogeneities are not a big limitation, as the wavelength is longer than the dimensions of the brain. Thus, RF volume coils such as birdcage coil or transverse electromagnetic (TEM) coils are frequently used.[9–12] However, at 7T and higher field MRI, those coils typically show a central brightening effect in the brain, with low transmit field at the edges of the brain, such as the temporal lobes.[5,13] Dielectric pads were proposed to address this issue but they only offer a limited and local improvement of the transmit field generated by volume coils.[14,15] Moreover, the quality (e.g the compound's properties) of dielectric pads could degrade over time and different head shapes or head movements can also impact its performances. Thus the capability to offer a large and efficient coverage of the head with a robust and reliable setup remains unsolved. Parallel transmit systems, where an array of multiple independent RF coils are used for the brain or body MR scans have been proposed to minimize such obstacles at ultra-high field. By modulating the RF phases and amplitudes[16] of each transmit element in the array, constructive transmit field (B_1^+) interferences can be generated over the region-of-interest (ROI), and thus improve signal homogeneity. Several RF coil array designs have been previously reported based on loop coils[17–20] or micro-strips[21,22] elements for human brain imaging and demonstrated good B_1^+ efficiencies in the cerebral cortex.

Dipole antennas were proposed as an alternative to loop coils as they were shown to have better RF signal penetration depth and field symmetry at 7T MRI.[25,26] With a center-shortened dipole antenna (where the shortening inductances were placed at the center) on a ceramic substrate, the strong electric fields were largely kept outside the subject tissues, and high B_1^+ field was achieved in deep body tissues. Thereafter, various others designs such as bow-tie (with the dipole placed on water-filled substrate), snake dipole, distributed inductance or dipole-loop configurations were investigated for body imaging.[27–30] In particular, a fractionated dipole design (where the two legs of the dipole are split and connected through lumped elements) without ceramic substrate demonstrated higher $B^+_{1,\text{in-depth}}/\sqrt{SAR_{10g,max}}$ compared to a center-shortened dipole with and without substrate.[31] This is why for body MR scans, the fractionated dipole was commonly adopted for coil array designs.[30–32] Making use of the properties previously stated, an RF coil array built with dipoles might be able to cover the auditory cortex, the cerebral lobes (frontal, occipital, parietal, temporal) and the cerebellum, either together, or with high B_1^+ field through RF phases optimization. Chen et al.[33] previously reported a dipole coil array for head imaging based on meander ends dipole and observed an extended coverage in the neck compared to a commercially available birdcage coil. However, due to the longitudinal extent of the coil array (dipoles' length = 320 mm), an excessive loading by the shoulders negatively affected the B_1^+ efficiency. By adapting the geometry of the coil array to cover specifically the whole-brain (cerebral cortex and cerebellum) higher B_1^+ efficiency might be achieved. Moreover, even though for body imaging, the fractionated dipole demonstrated better performance compared to the center-shortened dipole, it is still undetermined whether a center-shortened or fractionated dipole coil array design would be more suitable to achieve a B_1^+-efficient whole-brain coverage, as no comparison was yet been made. For body dipole coil arrays the individual properties of dipole designs (center-shortened or fractionated) might be extended to array configurations as the sufficient distance between neighbors allows for enough decoupling. But for a B_1^+-efficient imaging of the brain, a tight geometrical arrangement requires the dipoles to be positioned looking to each other, which will increase the coupling.

For body MRI, the better signal penetration depth of dipoles compared to loop coils has been clearly demonstrated beneficial but for brain MR imaging, reaching deep structures is not a main concern because of the limited size of the head. Nevertheless, the extended longitudinal coverage attained with dipoles might yield higher MR signal in challenging regions such as the cerebellum. However, the inter-element interaction can alter the fine tuning, and matching of the dipoles, and might induce field cancellations. Thus, the placement of the dipoles is a critical step to generate a high B_1^+ field. Therefore, the aim of the present study was to design, develop and evaluate an 8-channel dipole coil array able of providing whole coverage of the human brain with a high B_1^+ field for MR measurements at 7T.

2 | METHODS

2.1 | Single dipole design

A single center-shortened dipole and a fractionated dipole (170 mm long, 15 mm width, 12 mm gap between legs) were etched from 35 μm copper on a FR4 substrate with a thickness of 0.1 mm. For center-shortened dipole, hand-wound shielded-copper inductors (diameter = 1 mm, Rowan Cable Products Ltd, England) were placed close to the feeding point while for the fractionated dipole, each leg was split in two pieces with a 5 mm gap in between to place the inductors (Figure 1A). Non-magnetic capacitors (American Technical Ceramics, NY, USA) were used as additional lumped elements to match the dipoles to 50 Ohms at 297.2 MHz (7T). Then, a single center-shortened and fractionated dipole B_1^+ excitation profiles were experimentally measured. Thereafter, a dipole coil array was modeled and simulated for the center-shortened and the fractionated dipole designs.

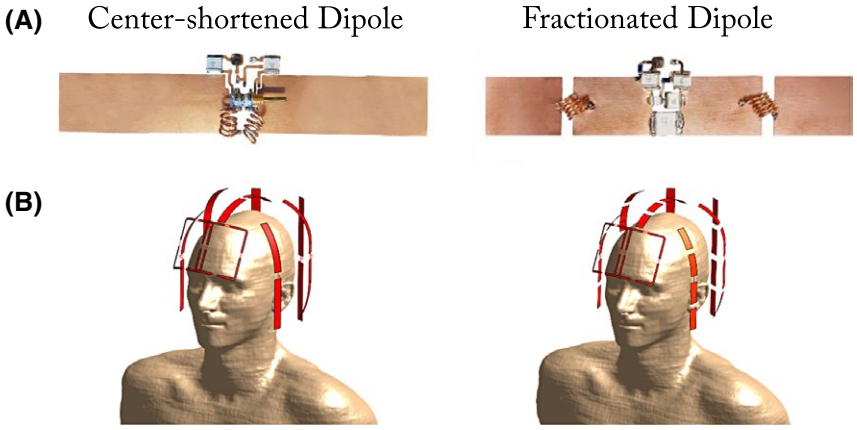

FIGURE 1 (A) Photos of the center-shortened and fractionated dipole designs. The inductors are placed in series and connected to each leg. They are used to tune the dipole at the right frequency by extending its electrical length. Three capacitors (2 in series, 1 in parallel) are used to match the dipole to 50 Ohms. (B) Simulation model for the 8-channel center-shortened/fractionated dipole coil arrays with frontal loops

2.2 | Coil array design

The center-shortened and fractionated dipoles for the arrays were modeled with lengths from 158.5 mm to 230 mm and 15 mm width, to ensure an efficient coverage of the head and a tight placement. For both dipole designs, the same geometrical arrangement was applied. Six dipoles were placed around the occipital and temporal lobes of the brain, arranged symmetrically (left-right) but non-uniformly centered along the longitudinal axis to account for the human brain geometry (Figure 1B). The dipoles 3 and 4, placed on the back side of the head, were centered closer to the cerebellum to provide higher signal in this region. A seventh dipole was placed around the parietal lobe and aligned in the anterior-posterior direction, perpendicular to the main magnetic field to provide high RF field at the top of the head where it is usually challenging to achieve high B_1^+ field (Figure 1B). The dipoles 1, 2, 5, 6 and 7 were slightly bent to follow the curvature of the head. Compared to placing dipoles at the frontal lobe, loop coils demonstrated higher B_1^+ efficiency and lower mutual coupling by coil overlapping. Thus, two 95×85 mm^2 loops were placed over the frontal region of the head and tilted.

2.3 | Electromagnetic field simulations

Both arrays were simulated with the finite-difference time-domain (FDTD) method on Sim4Life 3.4 (ZMT AG, Switzerland) on a whole body human model, Duke[34] (Figure 1B). All the coil array elements (dipoles and loops) were defined as perfect electric conductors (PEC), gridded at 3 mm-iso, and lumped elements were placed for tuning and matching. Moreover, a topological voxeler was used for the coils to guarantee that their geometry was correctly voxelised. The Duke model was gridded at 2 mm-iso and truncated below the torso to reduce the simulation time without impacting the area of interest (20 Mcells in total). All the coils were driven individually by a Gaussian excitation centered at 297.2 MHz with a 500 MHz bandwidth and computations were carried out on a dedicated GPU (2 × GTX 1080Ti, Nvidia Corp., USA) with an average simulation time of 1 hour per channel for a convergence better than −50 dB (quantifying the variations in the results between two consecutive iterations). An integrated match-tool was used to tune and match the resonant elements in post-processing by adapting the lumped element values which were then introduced into the simulation model. Both arrays were simulated including the inductor losses, modeled with series resistors, as calculated by Chen et al.[35] Absorbing boundary conditions were applied at the edges of the simulation space to ensure that no reflected wave would interfere with the forward electromagnetic wave.

All the results were interpolated at 1 mm-iso inside a virtual box ($200 \times 250 \times 230$ mm^3) surrounding the head of the human model and normalized to 1 W input power. When compared with experimental data, the simulations were corrected for the losses in the line till the coil array (more details are given in the paragraph about transmit field characterization). Individual B_1^+ maps and scattering matrices were exported to Matlab (2017a, the Mathworks, Natick, Massachusetts) to be processed. The $B_1^+/\sqrt{SAR_{10g,max}}$ maps were computed for individual center-shortened and fractionated dipoles in the array. Then, RF phases were optimized for two distinct areas, either whole-brain or cerebellum and the $B_1^+/\sqrt{SAR_{10g,max}}$ map was calculated for both center-shortened and fractionated dipole arrays. Thereafter, the center-shortened dipole array was built and further investigated as it demonstrated the best balance between RF performances, mechanical strength and ease of construction.

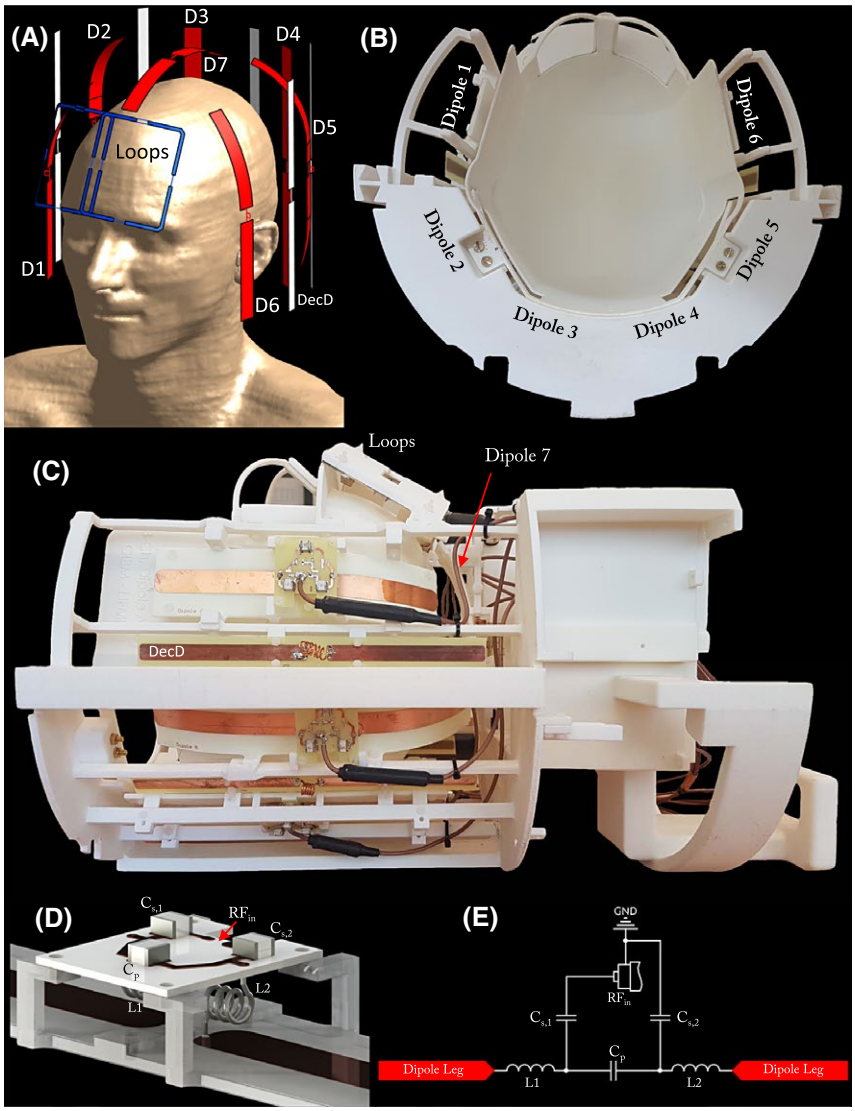

FIGURE 2 (A) Simulation model for the whole-brain center-shortened dipoles and frontal loops coil array. (B) and (C) Photos of the general design of the array. Six center-shortened dipoles were placed around occipital and temporal lobes (D1–D6) and one (D7) was placed around the parietal lobe. Two loop coils (1 and 2) were placed over the frontal lobe of the brain. (D) Isometric view of the feeding circuit, including the dipole, the tuning/matching circuit and the support structure for the dipole, and (E) corresponding schematics. $C_{s,1}$ and $C_{s,2}$ are capacitors, L1 and L2 are inductors placed in series with respect to the RF input and were mainly used to tune the dipole to 297.2 MHz. C_p is a capacitor connected between the two dipole's legs, in parallel of the RF input port and was mainly used to match the dipole to 50 Ohms

2.4 | Coil array construction

The center-shortened dipoles for the array were etched from 35 µm copper on a FR4 substrate with a thickness of 0.1 mm while the two loops were built with silver-plated copper wire. All geometrical dimensions, distances and placement were kept the same as in the simulated model. The RF feeding ports were placed at the center of the dipoles and connected to an in-house built transmit-receive switch with low noise preamplifiers (Stark Contrast, Erlangen, Germany) through 50 Ohms coaxial cables with equal phase length (diameter = 3 mm, Huber-Suhner, Switzerland). A single Tx power input was divided into quadrature and fed the two loops. Common-modes on the coaxial cables were diminished with a balun that is a quarter-wavelength transformer tuned to 297.2 MHz with capacitors. Tuning/matching to 297.2 MHz and S-parameter matrix measurement were performed using a 4-channel vector network analyser (Agilent Technologies 5071C-ENA Series, USA). To accommodate the shape of the human head, a helmet was designed with maximal dimensions in anterior-posterior direction equal to 222 mm, 187 mm from left to right and 231 mm from top to bottom. The whole structure was designed on Solidworks 2016 (Dassault Systems, France) and 3D printed (EOSINT P395, EOS, Germany) in nylon (EOS, PA2200) giving a maximal distance between the helmet and the RF coils of 15 mm (Figure 2B and C).

However, the center-shortened dipole design was more sensitive to high currents and voltages compared to other resonant coils as the inductors required to tune the dipoles were placed in the gap between the dipole legs. At resonance, electric arcs could occasionally occur between the inductors/capacitors and the dipole's legs, especially with power-intensive MR sequences. To avoid these side effects, the feeding line and the matching capacitors were soldered on a separate rigid PCB (0.8 mm thickness) placed 16 mm above the dipole (Figure 2D and E, $C_{s,1}$, $C_{s,2}$ and C_p). Then, the tuning inductors could be connected in between the rigid PCB and the

legs (Figure 2D and E, L1 and L2), which eliminated arcing, and provided high resistance to mechanical stress, particularly for adjustments of the inductor value.

The close distance between the dipoles (≈75 mm between the center of dipoles) placed around the head resulted in high couplings between neighbors. Thus, a decoupling method based on a magnetic wall approach was applied by placing a decoupling dipole (DecD) at equal distance between two dipoles, with no power input and with its legs short-circuited by an hand-wounded inductor adjusted to maximize the dipoles' isolation.[36] The DecDs (10 mm width, 12 mm gap between legs) were etched from 35 μm copper on a FR4 substrate with a thickness of 0.8 mm and a length equal to the mean length of the two dipoles in between which they were placed. Five DecDs were used between the dipoles 1 to 6 (Figure 2A, in white) and added to the simulation model, to account for their interactions with the dipoles.

2.5 | MR experiments

For a single center-shortened and a single fractionated dipole, measurements were performed on a spherical phantom (diameter ≈ 180 mm, Siemens D165-10606820) using a Magnetom 7T MR scanner with 8 x 1 kW RF amplifier (Step 1, Siemens, Erlangen, Germany). Measurements on the brain were acquired using the whole-brain center-shortened dipoles and frontal loop coil array (Magnetom 7T, Step 2.3).

2.6 | Particle-swarm optimization

In both phantom and human brain measurements, phase-only RF shimming was performed using a particle-swarm optimization (PSO) method.[37,38] Based on swarm intelligence, this iterative method aimed to minimize a cost function defined either for maximal B_1^+ field (Equation 1) or homogeneity (Equation 2).

$$\text{cost}_{\text{Maximal B1}} = \left(1 - \frac{\sum\sum_{i,j} Ratio(i,j)}{\text{Size}_{\text{ROI}}}\right) \times 100 \quad (1)$$

$$\text{cost}_{\text{Homogeneity}} = \alpha . \frac{1}{\left\langle B_1^+ \right\rangle_{\text{ROI}}} + \beta . \text{std}(B_{1,\text{ROI}}^+) \quad (2)$$

For maximal B_1^+ field (Equation 1), the Ratio(i,j) was defined as the ratio between the non-shimmed B_1^+ field and the sum-of-magnitudes for each pixel in the ROI, while for homogeneity (Equation 2) the cost function was defined as the weighted sum of the standard deviation and the inverse value of the mean B_1^+ field over the ROI. The weighting coefficients α and β could be adapted to balance B_1^+ efficiency and homogeneity. Using a multi-core processor (Intel Core i7-4790, 3.60 GHz), the convergence of the method was achieved in less than 20 seconds for maximal B_1^+ field and less than 40 s with the homogeneity cost function for any ROI considered.

2.7 | Transmit field characterization

All the B_1^+ maps were acquired with a SA2RAGE sequence for a 500 μs, 90°, 1 kW hard pulse.[39] To optimize the RF field in regions-of-interest (ROI), B_1^+ sensitivities (magnitude and phase) were extracted on Matlab, from a GRE-based sequence, and then processed with the PSO algorithm. The local SAR_{10g} maps were computed from the simulation results for the RF phases applied in measurements to evaluate the $B_1^+/\sqrt{SAR_{10g,max}}$ efficiency for such close-fitted dipole array. In phantom and human brain measurements, the B_1^+ field was normalized to 1 kW input peak-power per channel, while the homogeneity was evaluated with the standard deviation. The B_1^+ field was compared for single center-shortened and single fractionated dipole that were placed at a distance of 15 mm from the phantom. The transmit losses, were measured to 37% (Siemens, Erlangen, Germany) between the RF amplifiers and the coil plug and approximately to 13% from the TR switch connected at the coil plug and the coils.

2.8 | Anatomical images

Healthy male volunteers who had signed a written consent approved by the local ethics committee were imaged with the whole-brain center-shortened dipoles and frontal loops coil array (Figure 2) and with the safety parameters set to the worst-case scenario as evaluated from the Q-matrix,[39] for a simulated model with the decoupling dipoles and without the inductor losses. RF phases of the individual channels were optimized with the PSO method and the B_1^+ field of individual coils and RF shimmed B_1^+ maps were evaluated. To acquire MR images, a 3D turbo-spin echo (3D-TSE, TE/TR = 120/2000 ms, resolution = 0.8 × 0.8 × 0.8 mm^3, FOV = 210 × 210 mm^2, Turbo Factor = 60, GRAPPA = 2, TA = 10 min 28 s), MP2RAGE[41] and multi-slice GRE (TE/TR = 16/1000 ms, resolution = 0.3 × 0.3 × 3 mm^3, FA = 60°, slices = 8, FOV = 210 × 210 mm^2, GRAPPA = 2, TA = 5 min 34 s) sequences were used.

3 | RESULTS

Individual B_1^+ excitation patterns for center-shortened and fractionated (where the two legs were splitted and connected with inductors) dipoles in a phantom showed that while the center-shortened dipole yielded slightly higher B_1^+ field in deeper regions, the fractionated dipole provided larger longitudinal field coverage (Figure 3).

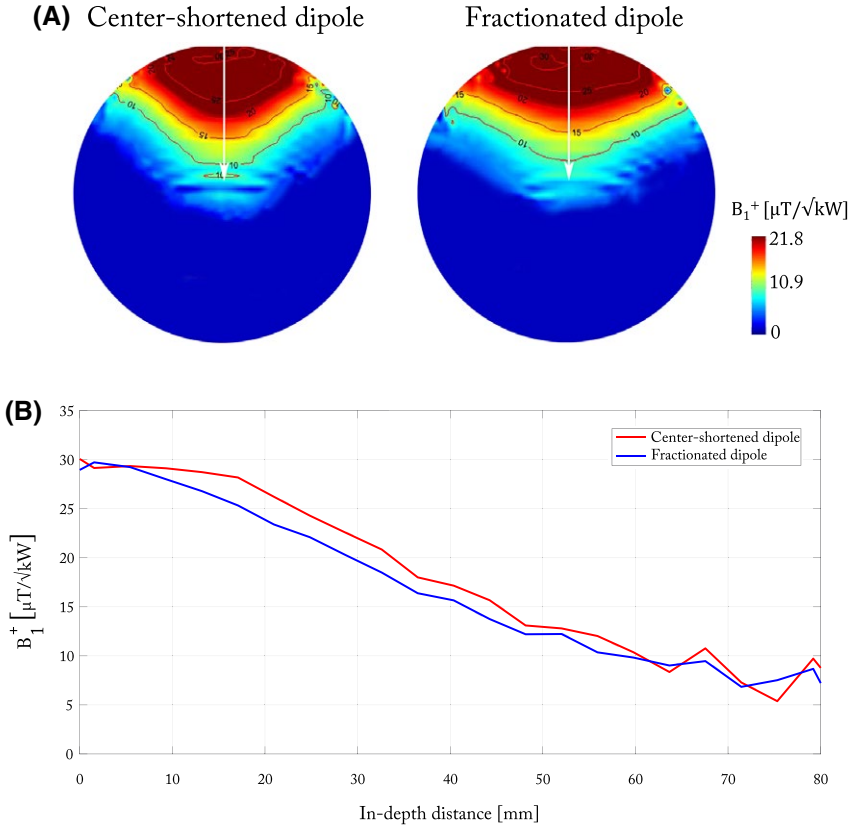

FIGURE 3 (A) Experimentally measured B_1^+ maps, normalized to 1 kW input power, along the dipole, for center-shortened and fractionated dipoles. Isolines are represented in red with their corresponding value inserted. (B) In-depth B_1^+ profiles for center-shortened and fractionated dipoles, taken along the white arrow visible in (A)

No significant differences were observed in $B_1^+/\sqrt{SAR_{10g,max}}$ maps, shown for individual center-shortened and fractionated dipole elements in the array (Figure 4A). Nevertheless, the individual fractionated dipoles in array demonstrated up to a 20% decrease in local $SAR_{10g,max}$ value compared to the center-shortened dipoles.

Over the mid-brain (transverse slice), the center-shortened dipole array showed a slightly better $B^+_{1,slice\text{-}mean}/\sqrt{SAR_{10g,max}}$ value compared to the fractionated dipole array (0.54 vs. $0.49\,\mu T\sqrt{kg}/\sqrt{W}$) while both dipole arrays had similar results over the whole head (less than 5% difference, Figure 4B). Specifically, with the center-shortened dipole array, higher $B^+_{1,in\text{-}depth}$-field and lower local $SAR_{10g,max}$ were observed. Over the mid-cerebellum (coronal slice), the fractionated dipole coil array showed a noticeably larger longitudinal coverage at similar $B^+_{1,cerebellum\text{-}mean}/\sqrt{SAR_{10g,max}}$ values ($0.57\,\mu T\sqrt{kg}/\sqrt{W}$ for center-shortened and $0.60\,\mu T\sqrt{kg}/\sqrt{W}$ for fractionated dipole array). However, better field penetration in depth was obtained with the center-shortened dipole array, particularly visible on sagittal view (Figure 4B). Nevertheless, as the differences between the two dipole arrays were marginal, only the 8-channel center-shortened dipole coil array was further investigated.

Measured S-matrix for the whole-brain center-shortened dipoles with frontal loops coil array demonstrated coupling values between neighbors and next neighbors below −15 dB for all the dipoles, which demonstrated the efficient isolation provided by the decoupling dipoles (Figure 5). Individually measured and simulated B_1^+ maps (Figure 6) were similar, and indicated a uniform transmit field distribution for the dipoles except for the dipole 1 which was visibly coupled to the closest loop. We note that the B_1^+-field for dipole 7 was quite efficient although it was placed perpendicular to the B_0 orientation.

To determine if the B_1^+ field coverage can be improved, B_1^+ RF fields were phase-shimmed in mid-brain (transverse slice) and the corresponding simulated $SAR_{10g,max}$, normalized to 1W input power was 0.69 W/kg (Figure 7A). A mean B_1^+ value of $28 \pm 2.3\,\mu T/\sqrt{kW}$ was measured over the shimmed ROI (Figure 8A, white solid line) while over a 3D volume encompassing the whole cerebral cortex (Figure 8A, white dashed rectangle), a mean B_1^+ value of $23.2 \pm 3.7\,\mu T/\sqrt{kW}$ was achieved. Nevertheless, the high-resolution 3D-TSE images demonstrated a whole-brain coverage with relatively good homogeneity across the slices in transverse and sagittal orientations (Figure 8B) while MP2RAGE images showed high homogeneity across multiples slices. High-resolution GRE images were acquired with the RF phases optimized in sagittal (Figure 9A) and transverse planes (Figure 9B) and demonstrated an homogeneous coverage of the whole-brain, including the cerebellum.

To evaluate the capability for the coil array to efficiently cover the deeper-lying brain regions, RF phase shimming was applied in mid-cerebellum coronal slice using the two different

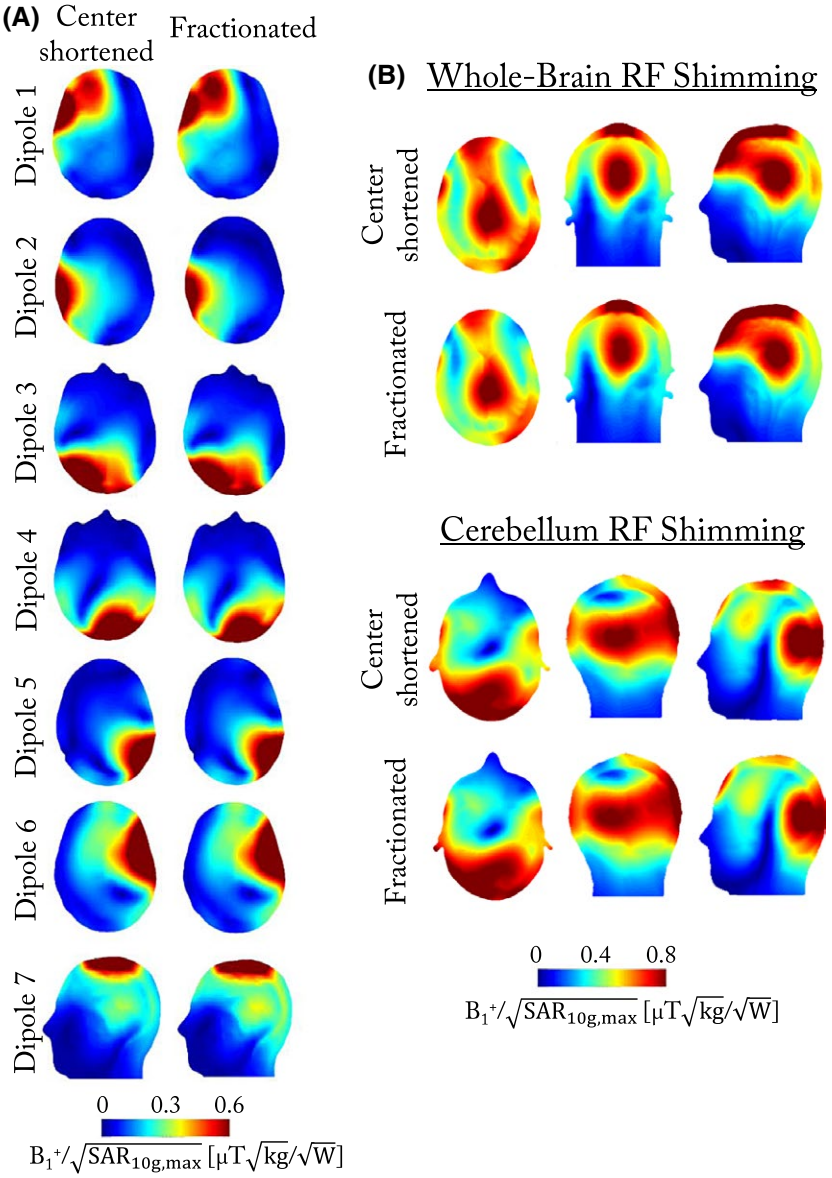

FIGURE 4 For the whole-brain center-shortened/fractionated dipole with frontal loops coil array, including the inductor losses: (A) simulated individual $B_1^+/\sqrt{SAR_{10g,max}}$ maps (B) simulated $B_1^+/\sqrt{SAR_{10g,max}}$ maps for RF phases optimized over whole-brain (upper maps) and cerebellum (bottom maps for maximal B_1^+ optimization)

cost functions, maximal B_1^+ field and homogeneity. As the ROI for phase optimization covered specifically the lower part of the brain, low transmit field was obtained in the upper regions. A mean B_1^+ value of $21 \pm 3.1\,\mu T/\sqrt{kW}$ was measured over a 3D volume encompassing the whole cerebellum (Figure 10A) for the maximal B_1^+ field optimization ($SAR_{10g,max} = 1.28$ W/kg, Figure 7B) and a mean B_1^+ value of $20.1 \pm 2\,\mu T/\sqrt{kW}$ was measured over the same volume for the homogeneous optimization. The high-resolution MP2RAGE (0.6 mm iso) images demonstrated a complete and relatively homogeneous coverage of the cerebellum (Figure 10B). On the edges of the cerebellum, the high-resolution 3D TSE (0.8 mm iso) image in coronal plane demonstrated the improvements achieved with the homogeneous goal (Figure 10B, red arrow) while B_1^+ field was not significantly decreased, and signal quality in the others directions (sagittal and transverse) was not visibly altered.

4 | DISCUSSION

In this study, a robust and reliable array configuration for whole-brain imaging was shown for an 8-channel center-shortened dipoles with a quadrature frontal loops coil array by B_1^+ maps and anatomical images with phase-only RF shimming. This conformal array design exploited the placement of center-shortened dipoles on the temporal, occipital and parietal lobes of the brain and two loop coils on the frontal lobe.

The geometrically adjusted conformal dipole coil array provided a homogeneous coverage of the cerebellum with less than 10% signal variation with RF phase-only shimming. Similar signal homogeneity was achieved in the cerebellum with an 8-channel microstrip Tx/15-channel Rx array covering the cerebellum.[42] However, while the longitudinal extent of this microstrip along the head was

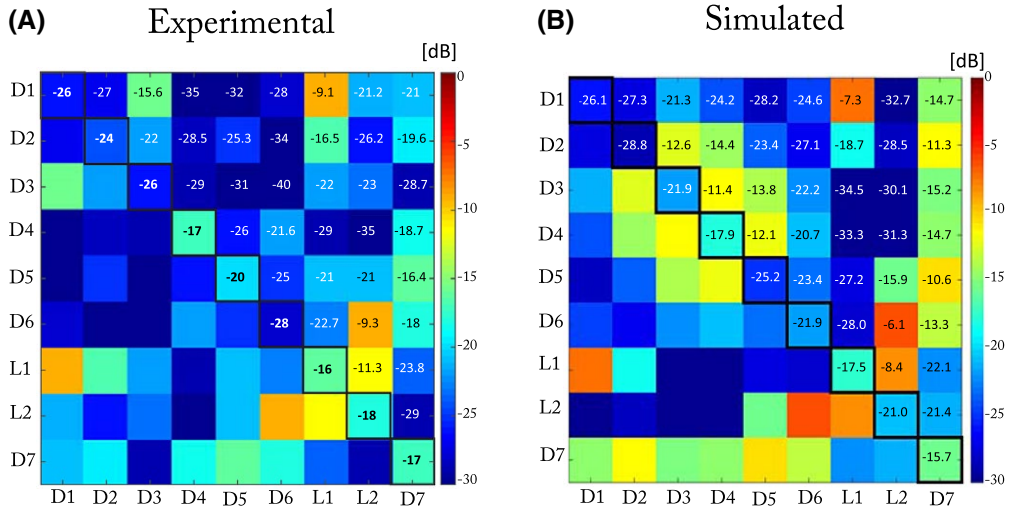

FIGURE 5 (A) Experimental and (B) simulated S-matrices for the whole-brain center-shortened dipoles and frontal loops coil array

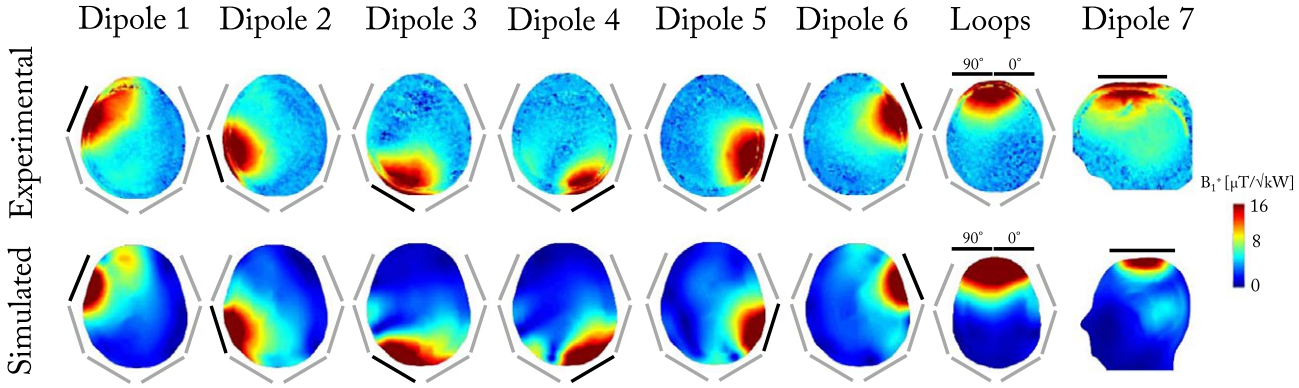

FIGURE 6 Experimentally measured (upper row) and simulated (bottom row) individual B_1^+ maps, normalized to 1 kW input power at the coil plug. The simulated maps were scaled for 50% losses. The transverse slice was taken in the midbrain region for dipoles 1 to 6 while the maximum slice was chosen for the loops and the middle sagittal slice for the dipole 7. In each map, the active coil is represented as a black line, for the whole-brain center-shortened dipoles and frontal loops coil array

310 mm long, our dipole array was designed in a way that dipole 3 and 4 were placed close to the cerebellum with a length of 220 mm. This might result in lower power input demand and consequently lower $SAR_{10g,max}$ values in the favor of the dipole array to achieve similar homogeneity. Notably, a 20% voltage input difference was measured in the cerebral and cerebellar regions to get a 90° flip angle with the dipole coil array. MR spectroscopy in cerebellum could greatly benefit from this result, as the power demand is usually higher compared to other MR applications. In comparison with the dipole coil array, a commercial single channel transmit/32-channel receive head coil (Nova Medical, USA) excited homogeneously the cerebral cortex with lower SAR restrictions. However, in the cerebellum region, the Nova coil demonstrated a clear lack of signal (see Supporting Information Figure S1).

The dipole coil array demonstrated the capability to cover simultaneously the cerebral and cerebellar regions in MR images. Therefore, both areas could be investigated in a single MR session without mechanical adjustments of the coil array. The transmit field efficiency reached by the dipole coil array competes with previously reported coil arrays at 7T[21,43–45] (within a 20% range) at the center of the brain. However, most of the 8-channel single-row coil arrays could not provide together whole-brain coverage and sufficient transmit field,[18,43] especially in the region of the cerebellum. Recently, a close fitting single-row coil array built with loop coils, was shown at 9.4T.[46] At similar B_1^+ efficiency at the cerebral cortex, the dipole coil array demonstrated a slightly higher $SAR_{10g,max}$ which lead to 17% lower $B^+_{1,mean}/\sqrt{SAR_{10g,max}}$ value. However, while the $SAR_{10g,max}$ value was observed in the brain for the dipole array, it is difficult to avoid the

$SAR_{10g,max}$ value close to the eyes for the loop array due to the conformal placement of the loops around the head. Moreover, a clear lack of signal could be observed in the cerebellum with this loop coil array. Therefore, 2×8 channels, distributed on two rows might lead to increased B_1^+ efficiency beyond the cerebral cortex.[17,18] In this study, we showed that the whole-brain coverage was achieved by the single row center-shortened dipoles and frontal loops coil array. However, even though good homogeneity could be achieved over relatively small regions, an asymmetric transmit field distribution was observed over larger areas such as whole cerebral cortex (Figure 8A). While phase-only RF shimming might be limited to optimize the homogeneity over large regions, other techniques such as strongly modulating pulses[47] or k_T-points could be used.[48,49]

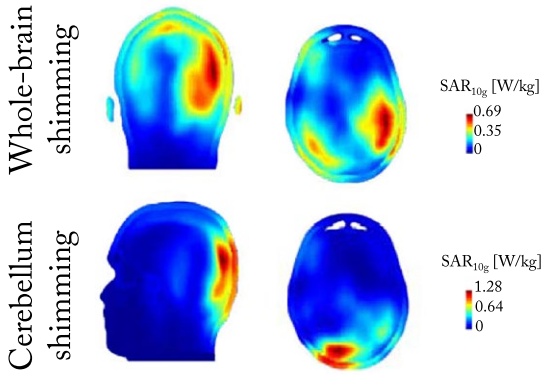

FIGURE 7 Local SAR_{10g} maps computed for the RF phases used in MR measurements and optimized for (A) whole-brain and (B) maximal B_1^+ in cerebellum. The maximum's slice was chosen and scaled to the corresponding $SAR_{10g,max}$ value. The simulation model did not include the inductor losses

Using decoupling dipoles is an useful method to decouple the close-fitting dipoles around the human head. A simple design of dipoles, tuned to the Larmor frequency with an inductor only enables decoupling of the dipoles in the array mostly lower than −20 dB in comparison to the decoupling value of −10 dB if no decoupling dipoles are present. Moreover, no decreased transmit field efficiency was observed in RF shimmed B_1^+ maps acquired with and without the DecDs. However, in the simulation model including the DecDs, the dipoles 2, 3 and 4 exhibited lower decoupling values compared to the measurements, which might be due to the absence of components (RF cables and baluns) and material losses in the simulated model. It also appeared in both the simulations and measured transmit field maps that despite a symmetrical placement of the dipoles, the dipole 1 is more affected by its closest loop (loop 1) than dipole 6 by loop 2. This behavior might be induced by a different field polarization from the dipoles placed either on left or right side of the head, but this needs to be further investigated.

As a fractionated dipole shows higher $B_1^+/\sqrt{SAR_{10g,max}}$ level compared to a center-shortened dipole at the depth of 5 cm and further,[31] it might be preferable to build coil arrays using fractionated dipoles. However, it appears that for close-fitted brain coil arrays this statement might not apply. The head size being considerably smaller compared to body regions, it requires a much tighter placement of the coil array elements. With our coil array design, even though the single fractionated dipoles in the array yielded lower

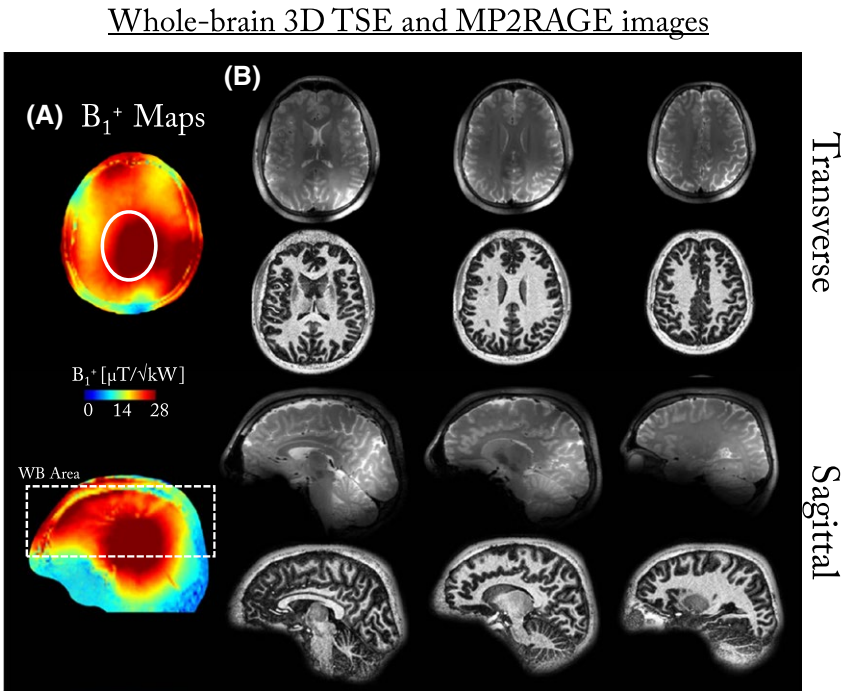

FIGURE 8 (A) RF phase-shimmed B_1^+ maps shown in transverse and sagittal plane, normalized to 1 kW input power per channel. Phase-only RF shimming was applied in the elliptical ROI (white solid lines) visible on transverse plane. A 3D region encompassing the whole cerebral cortex (white dashed rectangle in sagittal view) was selected to evaluate the B_1^+ efficiency across multiple slices (B) High-resolution 3D-TSE (first row, $0.8 \times 0.8 \times 0.8$ mm^3) and MP2RAGE (second row, $0.6 \times 0.6 \times 0.6$ mm^3) images displayed in transverse and sagittal planes for different slices with the RF phases applied in (A). No post-processing correction was applied

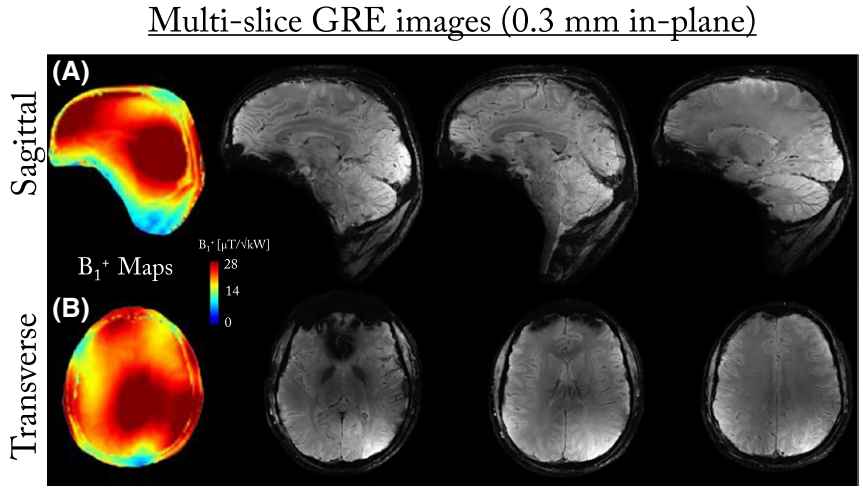

FIGURE 9 RF phase-shimmed B_1^+ maps, normalized to 1 kW input power per channel, and high-resolution GRE images (0.3×0.3 mm^2 in plane) for RF phases optimized in (A) sagittal and (B) transverse planes. No post-processing correction was applied

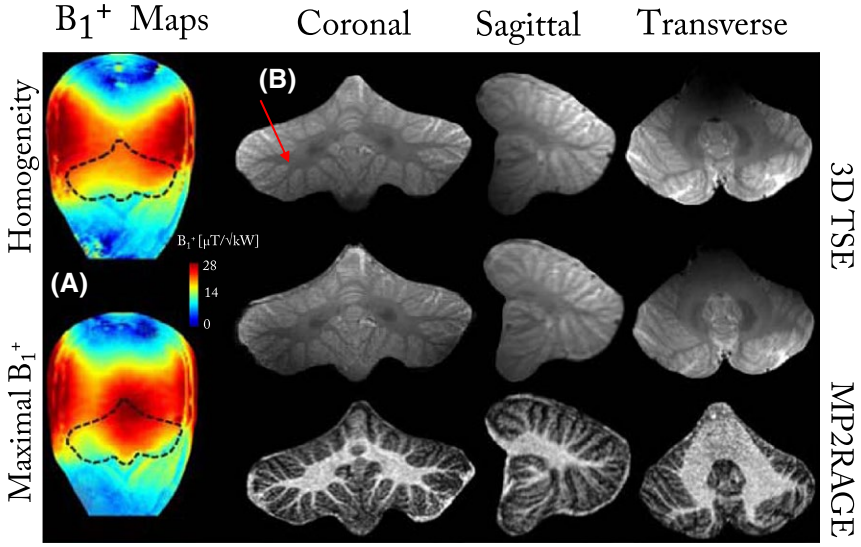

FIGURE 10 (A) Experimentally measured RF phase-shimmed B_1^+ maps, normalized to 1 kW input power per channel for the homogeneous and maximal B_1^+ cost functions. The cerebellum position is indicated for information (dashed black line) (B) High-resolution 3D TSE images ($0.8 \times 0.8 \times 0.8$ mm^3) and MP2RAGE ($0.6 \times 0.6 \times 0.6$ mm^3) images displayed in coronal, sagittal and transverse orientations for the RF phases applied in (A). The red arrow indicates the local improvement in signal homogeneity achieved with the homogeneous cost function. No post-processing correction was applied

SAR_{10g} levels compared to the center-shortened dipole in the array, the center-shortened dipole array offered comparable performances and could even perform slightly better in terms of $B_1^+/\sqrt{SAR_{10g,max}}$ ratio depending on the ROI chosen for RF phases optimization. Moreover, individual $B_1^+/\sqrt{SAR_{10g,max}}$ maps did not show significant differences between the center-shortened and fractionated dipoles (Figure 4A).

It might be beneficial to combine the 8-channel whole-brain center-shortened dipoles and frontal loops coil array with a multi receivers loop array to improve SNR and acquisition speed.[50,51] With the 8-channel dipole array, it might be possible to place e.g 32 independent receive loops between the dipoles and the head without increasing the dipoles' distance to the head or modifying their position. Then, this coil array could be used to perform studies, where timing of the acquisition and SNR are critical.[52] Another potential field of application for this coil array could be in arterial spin labelling (ASL). Introduced in 1992,[53] it aimed to measure the cerebral blood flow during brain activity. However, this method requires a inversion pulse to be applied on the neck region to "label" the inflowing water proton spins in the arterial blood. Thus, high B_1^+ efficiency is required in both brain and neck regions. With the coil array presented here, the idea is to simply replace the dipole 7 (placed on top of the head) by a single loop coil positioned over the neck and uniquely dedicated to apply the inversion pulse required by the ASL method.

5 | CONCLUSION

The *robust* and *structurally optimized* seven center-shortened dipoles with frontal loop coils array enabled whole-brain imaging, including cerebellum, with high transmit efficiency and RF homogeneity achieved with only RF phase shimming. The high B_1^+ efficiency achieved in cerebellum, combined with moderate SAR levels, would greatly benefit MR spectroscopy studies in this challenging region and the appreciable phase-only RF shimming qualities could contribute to enhance the robustness of fMRI data, particularly compared to single channel systems when the transmit field is too low. We conclude that the whole-brain center-shortened dipoles and frontal loop coil array represents a valuable contribution to MR applications at 7 Tesla.

ACKNOWLEDGMENTS

This study was supported by Centre d'Imagerie Biomedicale (CIBM) of the UNIL, UNIGE, HUG, CHUV, EPFL and the Leenaards and Jeantet Foundations.

REFERENCES

1. Hoult D, Richards R. The signal-to-noise ratio of the nuclear magnetic resonance experiment. *J Magn Reson.* 2011;213:329–343.
2. Vaughan J, Garwood M, Collins C, et al. 7t vs. 4t: Rf power, homogeneity, and signal-to-noise comparison in head images. *Magn Reso Med.* 2001;46:24–30.
3. Gruetter R, Weisdorf SA, Rajanayagan V, et al. Resolution improvements inin vivo1h nmr spectra with increased magnetic field strength. *J Magn Reson.* 1998;135:260–264.
4. Webb AG, Collins CM. Parallel transmit and receive technology in high-field magnetic resonance neuroimaging. *Int J Imaging Syst Technol.* 2010;20:2–13.
5. Collins CM, Liu W, Schreiber W, Yang QX, Smith MB. Central brightening due to constructive interference with, without, and despite dielectric resonance. *J Magn Reson Imaging.* 2005;21192–196.
6. Hoult DI. Sensitivity and power deposition in a high-field imaging experiment. *J Magn Reson Imaging.* 2000;12:46–67.
7. Collins CM, Liu W, Wang J, et al. Temperature and sar calculations for a human head within volume and surface coils at 64 and 300 mhz. *J Mag Reson Imaging.* 2004;19:650–656.
8. van Osch MJP, Webb AG. Safety of ultra-high field MRI: What are the specific risks? *Current Radiol Rep.* 2014;2:61.
9. Hayes C, Edelstein W, Schenck J, Mueller O, Eash M. An efficient, highly homogeneous radiofrequency coil for whole-body nmr imaging at 1.5t. *J Magn Reson.* 1985;63:622–628.
10. Wiggins GC, Potthast A, Triantafyllou C, Wiggins CJ, Wald LL. Eight-channel phased array coil and detunable tem volume coil for 7 t brain imaging. *Magn Reson Med.* 2005;54:235–240.
11. Vaughan J, Adriany G, Garwood M, et al. Detunable transverse electromagnetic (tem) volume coil for high-field NMR. *Magn Reson Med.* 2002;47:990–1000.
12. Mekle R, van der Zwaag W, Joosten A, Gruetter R. Comparison of three commercially vailable radio frequency coils for human brain imaging at 3 tesla. *Magn Reson Mater Phys Biol Med.* 2008;21:53.
13. Ipek O. Radio-frequency coils for ultra-high field magnetic resonance. *Anal Biochem.* 2017;529:10–16.
14. Snaar J, Teeuwisse W, Versluis M, et al. Improvements in high-field localized mrs of the medial temporal lobe in humans using new deformable high-dielectric materials. *NMR Biomed.* 2011;24:873–879.
15. Teeuwisse WM, Brink WM, Webb AG. Quantitative assessment of the effects of high-permittivity pads in 7 tesla mri of the brain. *Magn Reson Med.* 2012;67:1285–1293.
16. Metzger GJ, Snyder C, Akgun C, Vaughan T, Ugurbil K, Van de Moortele PF. Local b1+ shimming for prostate imaging with transceiver arrays at 7t based on subject-dependent transmit phase measurements. *Magn Reson Med.* 2008;59:396–409.
17. Shajan G, Kozlov M, Hoffmann J, Turner R, Scheffler K, Pohmann R. A 16-channel dual-row transmit array in combination with a 31-element receive array for human brain imaging at 9.4 t. *Magn Reson Med.*2014;71:870–879.
18. Avdievich NI. Transceiver-phased arrays for human brain studies at 7 t. *Appl Magn Reson.* 2011;41:483–506.
19. Yan X, Ma C, Shi L, et al. Optimization of an 8-channel loop-array coil for a 7 t MRI system with the guidance of a co-simulation approach. *Appl Magn Reson.* 2014;45:437–449.
20. Clement J, Ipek O, Eggenschwiler F, Donati G, Pierzchala K, Gruetter R. Eight-channel loop coil array for 7t MR brain imaging. In Proceedings of the 32nd Annual Meeting of ESMRMB, Edinburgh, United Kingdom, 2015;284.
21. Adriany G, Van de Moortele PF, Wiesinger F, et al. Transmit and receive transmission line arrays for 7 tesla parallel imaging. *Magn Reson Med.* 2005;53:434–445.
22. Yan X, Pedersen J, Wei L, Zhang X, Xue R. Multichannel double-row transmission line array for human mr imaging at ultrahigh fields. *IEEE Trans Biomed Eng.* 2015;62:1652–1659.
23. Röschmann P. Radiofrequency penetration and absorption in the human body: Limitations to high-field whole-body nuclear magnetic resonance imaging. *Med Phys.* 1987;14:922–931.
24. Raaijmakers AJE, Luijten PR, van den Berg CAT. Dipole antennas for ultrahigh-field body imaging: A comparison with loop coils. *NMR Biomed.* 2016;29:1122–1130. NBM-14-0331.R1.
25. Raaijmakers AJE, Ipek O, Klomp DWJ, et al. Design of a radiative surface coil array element at 7t: The single-side adapted dipole antenna. *Magn Reson Med.* 2011;66:1488–1497.
26. Ipek O, Raaijmakers A, Klomp D, Lagendijk J, Luijten P, Van den Berg C. Characterization of transceive surface elements designs for 7 tesla magnetic resonance imaging of the prostate: Radiative antenna and microstrip. *Phys Med Biol.* 2012;57.
27. Oezerdem C, Winter L, Graessl A, et al. 16-channel bow tie antenna transceiver array for cardiac mr at 7.0 tesla. *Magn Reson Med.* 2016;75:2553–2565.
28. Steensma B, Obando A, Klomp D, Van den Berg N, Luijten P, Raaijmakers A. Body imaging at 7 tesla with much lower sar levels: An introduction of the snake antenna array. In Proceedings of the 24th Annual Meeting of ISMRM, Singapore, 2016;395.

29. Wiggins G, Lakshmanan KGC. The distributed inductance electric dipole antenna. In Proceedings of the 23rd Annual Meeting of ISMRM, Toronto, Canada, 2015;3100.
30. Ertürk MA, Raaijmakers AJE, Adriany G, Uğurbil K, Metzger GJ. A 16-channel combined loop-dipole transceiver array for 7 tesla body MRI. *Magn Reson Med.* 2017;77:884–894.
31. Raaijmakers AJ, Italiaander M, Voogt IJ, et al. The fractionated dipole antenna: A new antenna for body imaging at 7 tesla. *Magn Reson Med.* 2016;75:1366–1374.
32. Voogt I, Klomp D, Hoogduin H, et al. Combined 8-channel transceiver fractionated dipole antenna array with a 16-channel loop coil receive array for body imaging at 7 Tesla. In Proceedings of the 23rd Annual Meeting of ISMRM, Toronto, Canada, 2015;631.
33. Chen G, Cloos M, Sodickson D, Wiggins G. A 7T 8 channel transmit-receive dipole array for head imaging: Dipole element and coil evaluation. In Proceedings of the 22nd Annual Meeting of ISMRM, Milan, Italy, 2014.
34. Gosselin M, Neufeld E, Moser H. Development of a new generation of high-resolution anatomical models for medical device evaluation: The virtual population 3.0. *Phys Med Biol.* 2014;59:5287.
35. Chen G, Collins C, Sodickson D, Wiggins G. A method to assess the loss of a dipole antenna for ultra-high-field MRI. *Magn Reson Med.* 2018;79:1773–1780.
36. Yan X, Zhang X, Wei L, Xue R. Design and test of magnetic wall decoupling for dipole transmit/receive array for mr imaging at the ultrahigh field of 7t. *Appl Magn Reson.* 2015;46:59–66.
37. Kennedy J, Eberhart RC. Particle swarm optimization. In Proceedings of the 1995 IEEE International Conference on Neural Networks, Perth, Australia, Piscataway, NJ: IEEE Service Center; 1995. pp. 1942–1948.
38. Clement J, Gruetter R, Ipek O. Comparison of passive RF phase shimming methods on the human brain at 7t using particle-swarm optimization. In Proceedings of the 33rd Annual Meeting of ESMRMB, Vienna, Austria, 2015;503.
39. Eggenschwiler F, Kober T, Magill AW, Gruetter R, Marques JP. Sa2rage: A new sequence for fast b1+-mapping. *Magn Reson Med.* 2012;67:1609–1619.
40. Ipek O, Raaijmakers AJ, Lagendijk JJ, Luijten PR, van den Berg CAT. Intersubject local sar variation for 7t prostate mr imaging with an eight-channel single-side adapted dipole antenna array. *Magn Reson Med.* 2014;71:1559–1567.
41. Marques JP, Kober T, Krueger G, van der Zwaag W, de Moortele PFV, Gruetter R. Mp2rage, a self bias-field corrected sequence for improved segmentation and t1-mapping at high field. *NeuroImage.* 2010;49:1271–1281.
42. Pfaffenrot V, Brunheim S, Rietsch SHG, et al. An 8/15-channel Tx/Rx head neck RF coil combination with region-specific B1+ shimming for whole-brain MRI focused on the cerebellum at 7T. *Magn Reson Med.* 2018;80:1252–1265.
43. Avdievich N, Pan J, Baehring J, Spencer D, Hetherington H. Short echo spectroscopic imaging of the human brain at 7t using transceiver arrays. *Magn Reson Med.* 2009;62:17–25.
44. Gilbert K, Belliveau JG, Curtis A, Gati J, Klassen M, Menon R. A conformal transceive array for 7 T neuroimaging. *Magn Reson Med.* 2011;67:1487–1496.
45. Adriany G, Van de Moortele PF, Ritter J, et al. A geometrically adjustable 16-channel transmit/receive transmission line array for improved RF efficiency and parallel imaging performance at 7 Tesla. *Magn Reson Med.* 2008;59:590–597.
46. Avdievich N, Hoffmann J, Shajan G, et al. Evaluation of transmit efficiency and SAR for a tight fit transceiver human head phased array at 9.4 T. *NMR Biomed.* 2017;30. NBM-16-0195.R1.
47. Boulant N, Mangin JF, Amadon A. Counteracting radio frequency inhomogeneity in the human brain at 7 tesla using strongly modulating pulses. *Magn Reson Med.* 2009;61:1165–1172.
48. Cloos MA, Boulant N, Luong M, et al. KT-points: Short three-dimensional tailored RF pulses for IP-angle homogenization over an extended volume. *Magn Reson Med.* 2012;67:72–80.
49. Eggenschwiler F, O'Brien KR, Gruetter R, Marques JP. Improving t2-weighted imaging at high field through the use of KT-points. *Magn Reson Med.* 2014;71:1478–1488.
50. Duan Q, Nair G, Gudino N, et al. A 7t spine array based on electric dipole transmitters. *Magn Reson Med.* 2015;74:1189–1197.
51. Rietsch SH, Orzada S, Quick HH. An 8tx/32rx rf coil for 7t UHF body MRI. In Proceedings of the 24th Annual Meeting of ISMRM, Singapore, 2016;2131.
52. Parrish TB, Gitelman DR, LaBar KS, Mesulam MM. Impact of signal-to-noise on functional MRI. *Magn Reson Med.* 2000;44:925–932.
53. Williams D, Detre J, Leigh J, Koretsky A. Magnetic resonance imaging of perfusion using spin inversion of arterial water. In Proceedings of the National Academy of Sciences of the United States of America; 1992;89:212–216.

SUPPORTING INFORMATION

Additional Supporting Information may be found in the online version of this article.

FIGURE S1 Experimentally measured $B_1^+/\sqrt{SAR_{10g,max}}$ maps in midbrain slice (transverse, upper row) and mid-cerebellum slice (transverse, bottom row) for: (A) the dipole coil array with RF phases optimized over whole-brain and for maximal B_1^+ field in the cerebellum. (B) a single channel birdcage coil (Nova Medical USA)

How to cite this article: Clément JD, Gruetter R, Ipek Ö. A human cerebral and cerebellar 8-channel transceive RF dipole coil array at 7T. *Magn Reson Med*. 2019;81:1447–1458. https://doi.org/10.1002/mrm.27476